CLEO CONF 96-12
ICHEP96 PA02-054

$\Lambda\overline{\Lambda}$ Production in Two-photon Interactions at CLEO

CLEO Collaboration

(July 19, 1996)

Abstract

We use the CLEO detector at the Cornell e^+e^- storage ring, CESR, to study the two-photon production of $\Lambda\overline{\Lambda}$. We report the first observation of $\gamma\gamma \to \Lambda\overline{\Lambda}$ in our analysis of $3.4\,\mathrm{fb}^{-1}$ of e^+e^- interactions. We present the cross-section for $\gamma\gamma \to \Lambda\overline{\Lambda}$ as a function of the $\gamma\gamma$ center of mass energy and compare it to that predicted by the quark-diquark model. We search for $\gamma\gamma \to \Sigma^{\mathrm{o}}\overline{\Sigma}^{\mathrm{o}}$ and $\gamma\gamma \to \Lambda\overline{\Sigma}^{\mathrm{o}}$ events and estimate their contribution to the observed $\Lambda\overline{\Lambda}$ yield. Contrary to our studies of $\gamma\gamma \to p\overline{p}$ that supported a quark-diquark model of baryon production, the measured $\gamma\gamma \to \Lambda\overline{\Lambda}$ cross-section appears to disagree with the prediction of this model.

C. P. Jessop,[1] K. Lingel,[1] H. Marsiske,[1] M. L. Perl,[1] S. F. Schaffner,[1] D. Ugolini,[1] R. Wang,[1] X. Zhou,[1] T. E. Coan,[2] V. Fadeyev,[2] I. Korolkov,[2] Y. Maravin,[2] I. Narsky,[2] V. Shelkov,[2] R. Stroynowski,[2] J. Staeck,[2] I. Volobouev,[2] J. Ye,[2] M. Artuso,[3] A. Efimov,[3] M. Gao,[3] M. Goldberg,[3] R. Greene,[3] F. Frasconi,[3] D. He,[3] S. Kopp,[3] G. C. Moneti,[3] R. Mountain,[3] Y. Mukhin,[3] S. Schuh,[3] T. Skwarnicki,[3] S. Stone,[3] X. Xing,[3] J. Bartelt,[4] S. E. Csorna,[4] V. Jain,[4] S. Marka,[4] A. Freyberger,[5] R. Godang,[5] D. Gibaut,[5] K. Kinoshita,[5] I. C. Lai,[5] P. Pomianowski,[5] S. Schrenk,[5] G. Bonvicini,[6] D. Cinabro,[6] L. Perera,[6] B. Barish,[7] M. Chadha,[7] S. Chan,[7] G. Eigen,[7] J. S. Miller,[7] C. O'Grady,[7] M. Schmidtler,[7] J. Urheim,[7] A. J. Weinstein,[7] F. Würthwein,[7] D. M. Asner,[8] D. W. Bliss,[8] W. S. Brower,[8] G. Masek,[8] H. P. Paar,[8] M. Sivertz,[8] J. Gronberg,[9] C. M. Korte,[9] D. J. Lange,[9] R. Kutschke,[9] S. Menary,[9] R. J. Morrison,[9] S. Nakanishi,[9] H. N. Nelson,[9] T. K. Nelson,[9] C. Qiao,[9] J. D. Richman,[9] D. Roberts,[9] A. Ryd,[9] H. Tajima,[9] M. S. Witherell,[9] R. Balest,[10] B. H. Behrens,[10] K. Cho,[10] W. T. Ford,[10] H. Park,[10] P. Rankin,[10] J. Roy,[10] J. G. Smith,[10] J. P. Alexander,[11] C. Bebek,[11] B. E. Berger,[11] K. Berkelman,[11] K. Bloom,[11] D. G. Cassel,[11] H. A. Cho,[11] D. M. Coffman,[11] D. S. Crowcroft,[11] M. Dickson,[11] P. S. Drell,[11] R. Ehrlich,[11] R. Elia,[11] A. D. Foland,[11] P. Gaidarev,[11] R. S. Galik,[11] B. Gittelman,[11] S. W. Gray,[11] D. L. Hartill,[11] B. K. Heltsley,[11] P. I. Hopman,[11] S. L. Jones,[11] J. Kandaswamy,[11] N. Katayama,[11] P. C. Kim,[11] D. L. Kreinick,[11] T. Lee,[11] Y. Liu,[11] G. S. Ludwig,[11] J. Masui,[11] J. Mevissen,[11] N. B. Mistry,[11] C. R. Ng,[11] E. Nordberg,[11] M. Ogg,[11,*] J. R. Patterson,[11] D. Peterson,[11] D. Riley,[11] A. Soffer,[11] C. Ward,[11] P. Avery,[12] M. Athanas,[12] C. D. Jones,[12] M. Lohner,[12] C. Prescott,[12] S. Yang,[12] J. Yelton,[12] J. Zheng,[12] G. Brandenburg,[13] R. A. Briere,[13] D. Y.-J. Kim,[13] T. Liu,[13] M. Saulnier,[13] R. Wilson,[13] H. Yamamoto,[13] T. E. Browder,[14] F. Li,[14] Y. Li,[14] J. L. Rodriguez,[14] T. Bergfeld,[15] B. I. Eisenstein,[15] J. Ernst,[15] G. E. Gladding,[15] G. D. Gollin,[15] E. Johnson,[15] I. Karliner,[15] M. Palmer,[15] M. Selen,[15] J. J. Thaler,[15] K. W. Edwards,[16] A. Bellerive,[17] D. I. Britton,[17] R. Janicek,[17] D. B. MacFarlane,[17] K. W. McLean,[17] P. M. Patel,[17] A. J. Sadoff,[18] R. Ammar,[19] P. Baringer,[19] A. Bean,[19] D. Besson,[19] D. Coppage,[19] C. Darling,[19] R. Davis,[19] N. Hancock,[19] S. Kotov,[19] I. Kravchenko,[19] N. Kwak,[19] S. Anderson,[20] Y. Kubota,[20] M. Lattery,[20] J. J. O'Neill,[20] S. Patton,[20] R. Poling,[20] T. Riehle,[20] A. Smith,[20] V. Savinov,[20] M. S. Alam,[21] S. B. Athar,[21] Z. Ling,[21] A. H. Mahmood,[21] H. Severini,[21] S. Timm,[21] F. Wappler,[21] A. Anastassov,[22] S. Blinov,[22,†] J. E. Duboscq,[22] R. Fulton,[22] D. Fujino,[22] K. K. Gan,[22] T. Hart,[22] K. Honscheid,[22] H. Kagan,[22] R. Kass,[22] J. Lee,[22] M. Sung,[22] A. Undrus,[22,†] R. Wanke,[22] A. Wolf,[22] M. M. Zoeller,[22] B. Nemati,[23] S. J. Richichi,[23] W. R. Ross,[23] P. Skubic,[23] M. Wood,[23] M. Bishai,[24] J. Fast,[24] E. Gerndt,[24] J. W. Hinson,[24] D. H. Miller,[24] E. I. Shibata,[24] I. P. J. Shipsey,[24] M. Yurko,[24] L. Gibbons,[25] S. D. Johnson,[25] Y. Kwon,[25] S. Roberts,[25] and E. H. Thorndike[25]

[1]Stanford Linear Accelerator Center, Stanford University, Stanford, California 94309
[2]Southern Methodist University, Dallas, Texas 75275
[3]Syracuse University, Syracuse, New York 13244

---

[*]Permanent address: University of Texas at Austin.

[†]Permanent address: BINP, RU-630090 Novosibirsk, Russia.

[4]Vanderbilt University, Nashville, Tennessee 37235
[5]Virginia Polytechnic Institute and State University, Blacksburg, Virginia 24061
[6]Wayne State University, Detroit, Michigan 48202
[7]California Institute of Technology, Pasadena, California 91125
[8]University of California, San Diego, La Jolla, California 92093
[9]University of California, Santa Barbara, California 93106
[10]University of Colorado, Boulder, Colorado 80309-0390
[11]Cornell University, Ithaca, New York 14853
[12]University of Florida, Gainesville, Florida 32611
[13]Harvard University, Cambridge, Massachusetts 02138
[14]University of Hawaii at Manoa, Honolulu, Hawaii 96822
[15]University of Illinois, Champaign-Urbana, Illinois 61801
[16]Carleton University, Ottawa, Ontario, Canada K1S 5B6
and the Institute of Particle Physics, Canada
[17]McGill University, Montréal, Québec, Canada H3A 2T8
and the Institute of Particle Physics, Canada
[18]Ithaca College, Ithaca, New York 14850
[19]University of Kansas, Lawrence, Kansas 66045
[20]University of Minnesota, Minneapolis, Minnesota 55455
[21]State University of New York at Albany, Albany, New York 12222
[22]Ohio State University, Columbus, Ohio 43210
[23]University of Oklahoma, Norman, Oklahoma 73019
[24]Purdue University, West Lafayette, Indiana 47907
[25]University of Rochester, Rochester, New York 14627

Two-photon interactions are an interesting laboratory for studying quantum chromodynamics. The two-photon interactions observed at CLEO generally lie in a regime near the boundary where perturbative calculations are valid. The two-photon production cross-section for $\gamma\gamma \to p\overline{p}$, previously measured by CLEO [1], was consistent with the prediction of the quark-diquark model [2–4]. We extend that study of the two-photon production of baryons by measuring the cross-section for the production of $\gamma\gamma \to \Lambda\overline{\Lambda}$. Unlike the $\gamma\gamma \to p\overline{p}$ measurement, the measurement presented in this paper appears to disagree with the prediction of the model.

CLEO II is a general purpose detector [5] located at the e^+e^- storage ring, CESR [6], operating at $\sqrt{s} \sim 10.58$ GeV. CLEO II contains three concentric wire chambers that detect charged particles over 95% of the solid angle. Particle identification is performed using specific ionization energy loss (dE/dx) in the outer wire chamber. A superconducting solenoid provides a magnetic field of 1.5 T, giving a momentum resolution of $\sigma_p/p \approx [(0.15p/(\mathrm{GeV/c}))^2 + (0.5)^2]^{1/2}\%$. Outside of the wire chambers and a time of flight system, but inside the solenoid, is a CsI electromagnetic calorimeter, consisting of 7800 crystals arranged as two endcaps and a barrel region. For electromagnetic showers in the barrel, the calorimeter achieves an energy resolution of $\sigma_E/E \approx \{0.35/(E/\mathrm{GeV})^{0.75} + 1.9 - 0.1E/\mathrm{GeV}\}\%$.

The quark-diquark model [2–4] includes nonperturbative effects through the use of the diquark, a qq bound state within the baryon. With this model the authors are able to calculate cross-sections at lower values of W than is possible with a pure quark scheme [7]. Here W is the center of mass energy of the two photons. In the energy regime near threshold, the quark-diquark model is also expected to fail as effects not included in the model, such as higher order terms in the perturbation expansion, vector meson dominance, and effects of the baryon mass, come into play.

Signal and background two-photon Monte Carlo events were generated using the same program that was used in the $p\overline{p}$ analysis. The Monte Carlo event generator is based on the BGMS formalism [8]. The simulation of the transport and decay of the final state particles through the CLEO detector is performed by a GEANT [9] based detector simulator. The same analysis is applied to data and Monte Carlo events.

Kinematics of two-photon events are strongly influenced by the fact that the initial state photons tend to have a large fraction of their momenta along the beam line; that is, they are approximately real. A typical photon $|q^2|$ is $20\,\mathrm{MeV}^2$. Here q is the photon four-momentum. In particular, the electron and positron rarely have enough transverse momentum to be observed. In addition, due to the $\sim 1/E_\gamma$ spectrum of the photon production, the two photons rarely have the same magnitude of momentum. Consequently, the $\Lambda\overline{\Lambda}$ center of mass tends to be boosted along the beam axis. The decay products, $p\pi^-\overline{p}\pi^+$, usually have relatively low transverse momentum since the available energy in the Λ decay is relatively small, and the $\gamma\gamma \to \Lambda\overline{\Lambda}$ cross-section is strongly peaked near the $\Lambda\overline{\Lambda}$ threshold. We detect those events in which the decay products have sufficient transverse momentum for all four hadron tracks to be observed in CLEO. We do not search for detected electrons or positrons.

In our analysis of $3.4\,\mathrm{fb}^{-1}$ of data, we use the following selection criteria to minimize background. We select 4 track events in which the charge sum is zero. Both the proton and antiproton are required to pass dE/dx particle identification. We require that the event energy is less than 6.0 GeV and that the transverse component of the sum of the track momenta is less than 0.6 GeV/c. We veto events in which the candidate Λ or $\overline{\Lambda}$ vertex is

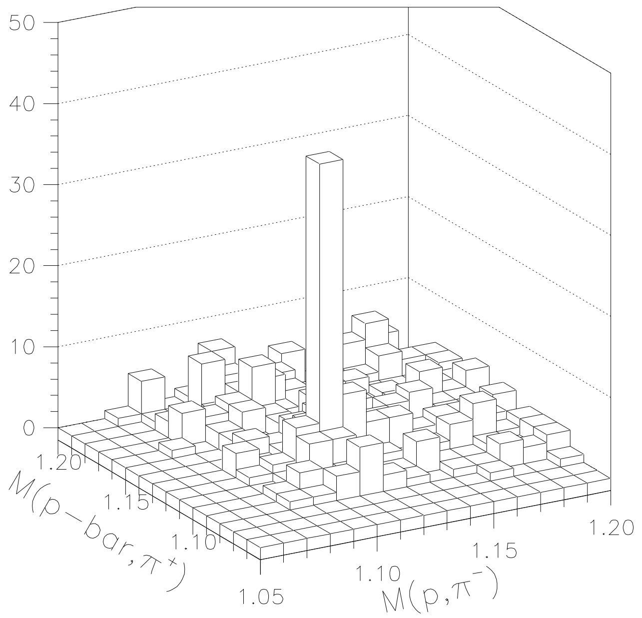

FIG. 1. $m_{p\pi^-}$ versus $m_{\overline{p}\pi^+}$, data

at the beam pipe. We also place a requirement on the transverse impact parameters of the constructed Λ and $\overline{\Lambda}$; the root sum square of the transverse impact parameters of Λ and $\overline{\Lambda}$, $(b_\Lambda^2 + b_{\overline{\Lambda}}^2)^{1/2}$, must be less than 1 cm. Finally, the theoretical predictions were made for the integrated cross-section up to $|\cos\theta^*| < 0.6$, where θ^* is the angle between the final state particle, here a Λ, and the two-photon axis in the two-photon center of mass. In order to compare with theory and previous $\gamma\gamma \to p\overline{p}$ measurements, we impose the same requirement on the data. To a good approximation, the two-photon axis is the beam axis as $|q^2|$ for the photons is small. We do not lose a significant number of signal events due to this selection criteria, since the acceptance of the detector decreases quickly beyond $|\cos\theta^*| = 0.6$. After applying these selection criteria we see a clear enhancement of the $\Lambda\overline{\Lambda}$ signal by plotting $m_{p\pi^-}$ versus $m_{\overline{p}\pi^+}$ in Figure 1. The small amount of background seen in data is consistent with non-resonant $\gamma\gamma \to p\pi^-\overline{p}\pi^+$.

The reconstructed particles are predominantly Λ's and $\overline{\Lambda}$'s produced in two-photon interactions. To demonstrate this, a number of data and Monte Carlo distributions have been compared, including event energy, radial decay distance, $\cos\theta^*$, proper decay length, acoplanarity, acolinearity, proton momentum and pion momentum distributions. In all cases there is good agreement between data and Monte Carlo generated distributions.

We use the Λ, $\overline{\Lambda}$ mass average, $(m_{p\pi^-} + m_{\overline{p}\pi^+})/2$, to measure the number of signal events. Viewed geometrically, the mass average rotates the $(m_{p\pi^-}, m_{\overline{p}\pi^+})$ plane by $-\pi/4$ and then scales it by $1/\sqrt{2}$; see Figure 2. The advantage of this approach is that it naturally maps the three types of backgrounds that concern us, Λ-fake, fake-$\overline{\Lambda}$, and fake-fake, into smooth backgrounds in the mass average plot which are easy to subtract when fitting.

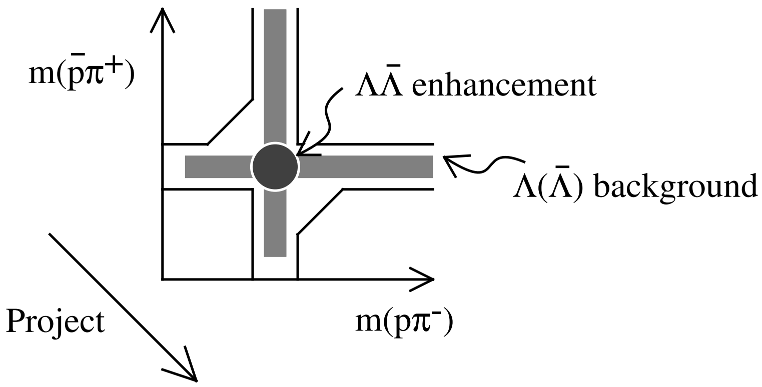

FIG. 2. $m_{p\pi^-}, m_{\overline{p}\pi^+}$ projection schematic

We reduce the fake-fake background by making a geometric cut on the $m_{p\pi^-}, m_{\overline{p}\pi^+}$ plot before the projection. We cut around the Λ mass on both axes, forming a modified cross in the $m_{p\pi^-}, m_{\overline{p}\pi^+}$ plane. As the width of the cross is larger than the width of Λ, this will not affect the signal. We use a cross-cut half-width of 6 MeV, which is several standard deviations in Λ mass resolution as observed in data. A simple cross geometry would underestimate fake-fake background near the $\Lambda\overline{\Lambda}$ point. To compensate for this, we extend our geometric cut at the intersection of the cross so that the area in the projected direction is a constant. This approach is valid since the background does not vary significantly across the cut. As can be observed in Figure 1, the non-resonant background is relatively smooth over the region of interest.

As we are less sensitive to other channels, we expect that the dominant portion of the observed $\Lambda\overline{\Lambda}$ yield is the two-photon production of $\Lambda\overline{\Lambda}$, $\Sigma^o\overline{\Sigma}^o$, $\Lambda\overline{\Sigma}^o$, and $\Sigma^o\overline{\Lambda}$. In order to measure the $\gamma\gamma \to (\Lambda/\Sigma^o)(\overline{\Lambda}/\overline{\Sigma}^o)$ cross-section as a function of $m_{\Lambda\overline{\Lambda}}$ we apply the projection technique to data and Monte Carlo events using the selection criteria discussed above, with the addition that we bin in $m_{\Lambda\overline{\Lambda}}$, where $m_{\Lambda\overline{\Lambda}}$ is the effective mass of the Λ and the $\overline{\Lambda}$. If the source of the signal is $\gamma\gamma \to \Lambda\overline{\Lambda}$, then $m_{\Lambda\overline{\Lambda}} = W$. At this point we have not used final state photon information so the produced states could be $\Lambda\overline{\Lambda}$, $\Lambda\overline{\Sigma}^o$, $\Sigma^o\overline{\Lambda}$, or $\Sigma^o\overline{\Sigma}^o$. We use the parenthetical notation to indicate alternative processes in which the observed $\Lambda\overline{\Lambda}$ pair may have been produced.

We fit to the background excluding the signal region, and subtract this from the number of events counted within the signal region, where we define the signal region to be within ~ 3 standard deviations of the Λ mass. Finally, we scale the measured signal using equation 1 to account for photon flux, efficiency, and the ratio of data to Monte Carlo luminosities. The results are displayed in Table I.

$$\sigma^{data}_{\gamma\gamma\to\Lambda\overline{\Lambda},m_{\Lambda\overline{\Lambda}}bin} \approx \frac{n^{data}_{bin}/L_{data}}{n^{MC}_{bin}/L_{MC,\Lambda\overline{\Lambda}}}\sigma^{MC}_{\gamma\gamma\to\Lambda\overline{\Lambda},m_{\Lambda\overline{\Lambda}}bin} \tag{1}$$

To calculate the $e^+e^- \to e^+e^-(\Lambda/\Sigma^o)(\overline{\Lambda}/\overline{\Sigma}^o)$ cross-section we apply the mass average technique for events that pass the selection criteria over all values of $m_{\Lambda\overline{\Lambda}}$. Using the Monte Carlo signal shape combined with a linear background, we measure 48.1 ± 8.3 events in data. To determine the overall efficiency we measure efficiency in bins of $m_{\Lambda\overline{\Lambda}}$ and weight each bin appropriately using data, giving an overall value of $(1.9 \pm 0.4 \pm 0.5)\%$, where the first error

TABLE I. Two-photon cross-sections, $|\cos\theta^*| < 0.6$, $\gamma\gamma \to (\Lambda/\Sigma^o)(\overline{\Lambda}/\overline{\Sigma}^o)$ and $\gamma\gamma \to \Lambda\overline{\Lambda}$ with $(\Sigma^o/\overline{\Sigma}^o)$ subtraction

$m_{\Lambda\overline{\Lambda}}$ [GeV]	$\sigma_{\gamma\gamma\to(\Lambda/\Sigma^o)(\overline{\Lambda}/\overline{\Sigma}^o)}$ [nb]	$\sigma_{\gamma\gamma\to\Lambda\overline{\Lambda}}$ [nb]
$2.25-2.4$	$6.3 \pm 2.2 \pm 2.2$	$4.3 \pm 1.9 \pm 1.7$
$2.4-2.5$	$1.5 \pm 0.6 \pm 0.4$	$1.0 \pm 0.5 \pm 0.3$
$2.5-2.6$	$0.87 \pm 0.38 \pm 0.24$	$0.60 \pm 0.31 \pm 0.19$
$2.6-2.9$	$0.36 \pm 0.09 \pm 0.10$	$0.25 \pm 0.09 \pm 0.08$
$2.9-3.6$	$0.056 \pm 0.022 \pm 0.015$	$0.039 \pm 0.019 \pm 0.012$

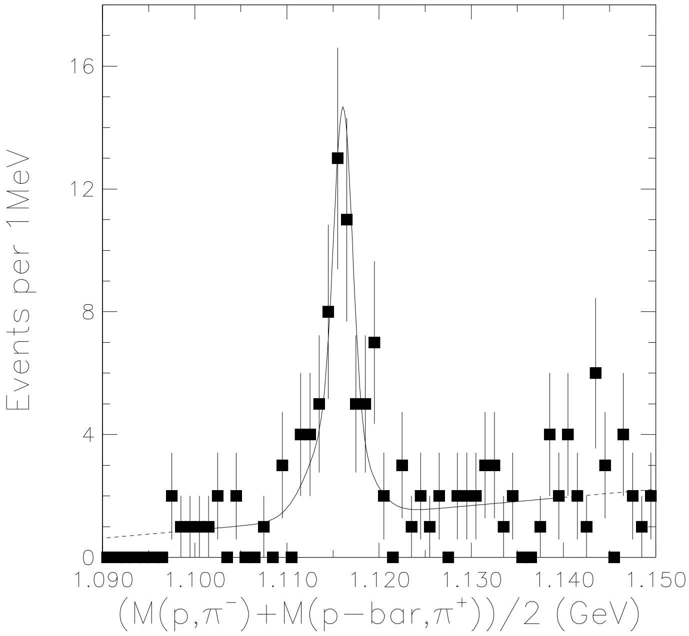

FIG. 3. $\Lambda\overline{\Lambda}$ mass average, $(m_{p\pi^-} + m_{\overline{p}\pi^+})/2$

is the uncertainty associated with correctly weighting the efficiency and the second error is the systematic uncertainty. This gives us an $e^+e^- \to e^+e^-(\Lambda/\Sigma^o)(\overline{\Lambda}/\overline{\Sigma}^o)$ cross-section for $|\cos\theta^*_\Lambda| < 0.6$ of $1.9 \pm 0.3 \pm 0.6$ pb, where the first error is statistical and the second error is due to the combined uncertainties of the efficiency. The fit and data are displayed in Figure 3.

The statistical uncertainty for the cross-section measurement of $\gamma\gamma \to (\Lambda/\Sigma^o)(\overline{\Lambda}/\overline{\Sigma}^o)$ is $\sim 40\%$ for each $m_{\Lambda\overline{\Lambda}}$ bin used in Table I. The statistical uncertainty in the cross-section measurement of $e^+e^- \to e^+e^-(\Lambda/\Sigma^o)(\overline{\Lambda}/\overline{\Sigma}^o)$ is only $\sim 17\%$. However, the uncertainty attributed to the efficiency due to $m_{\Lambda\overline{\Lambda}}$ distribution uncertainty is $\sim 23\%$. These large uncertainties set the scale of our concern for the systematic uncertainties. We have estimated the systematic uncertainty associated with binning, selection criteria, and background shape. The dominant sources of uncertainty are tracking, $\sim 14\%$, and triggering, $\sim 16\%$, which, combined in quadrature with the other sources of systematic uncertainty, gives 25%; see Table II.

TABLE II. Summary of systematic errors

Source	Error
Tracking	14%
Level 2 trigger	12%
Level 3 trigger	10%
Cross-cut	9%
Energy	6%
Transverse momentum	6%
Beampipe veto	4%
$\cos\theta^*$	4%
Particle ID	3%
Background shape	3%
Impact	2%
Total	25%

Due to reduced sensitivity to other channels combined with the steep W dependence of two-photon production, we expect that the dominant source of feeddown into the observed signal comes from the two-photon production of $\Sigma^o\overline{\Sigma}^o$, $\Lambda\overline{\Sigma}^o$ or $\Sigma^o\overline{\Lambda}$. As a result of the fact that antiprotons, and to a lesser extent the other hadrons, interact within the crystals of the CLEO calorimeter producing split-off showers, the $\sim$70 MeV photons from the Σ^o decay are difficult to identify. Due to the limited statistics, we do not use the mass average technique, but instead we proceed along a less ambitious path of looking for either a $(\Sigma^o/\overline{\Sigma}^o)$ in the events that pass all $\Lambda\overline{\Lambda}$ selection cuts described above and that lie within a 6 MeV radius of the $\Lambda\overline{\Lambda}$ point in the $(m_{p\pi^-}, m_{\overline{p}\pi^+})$ plane, where we use the notation $(\Sigma^o/\overline{\Sigma}^o)$ to indicate either Σ^o or $\overline{\Sigma}^o$. To search for $(\Sigma^o/\overline{\Sigma}^o)$ we combine each Λ or $\overline{\Lambda}$ with selected photon candidates in the event.

The following is a list of selection criteria we apply to the candidate photons. We only consider photon candidates in the crystal barrel, as the barrel region of the crystal detector has better energy resolution and fewer background photon candidates. The energy associated with the photon candidate must be within the range 40 MeV to 180 MeV. Each candidate photon must not be associated with an observed charged track, and we apply a stricter requirement that a candidate photon must be a large distance away from the shower associated with the anti-proton, $\cos\theta_{\gamma,\overline{p}} < 0.9$. To reduce background from hadronic interactions, we require that the ratio of energy deposited in closest 9 crystals to the energy deposited in the closest 25 crystals must be > 0.9.

For each $(\Sigma^o/\overline{\Sigma}^o)$ we construct the value of $m_{p,\pi,\gamma} - m_{p,\pi} + m_\Lambda$, the mass difference, with the constant m_Λ added so that the ideal $(\Sigma^o/\overline{\Sigma}^o)$ candidate would have a value equal to the Σ^o mass; see Figure 4. Using the Monte Carlo signal shape combined with a linear background to fit the data, we measure the number of $(\Sigma^o/\overline{\Sigma}^o)$ to be 9.5 ± 5.5. As the statistical error associated with this measurement is very large, we expect the systematic error to contribute little to the overall uncertainty, with the possible exception of interpretation which will be

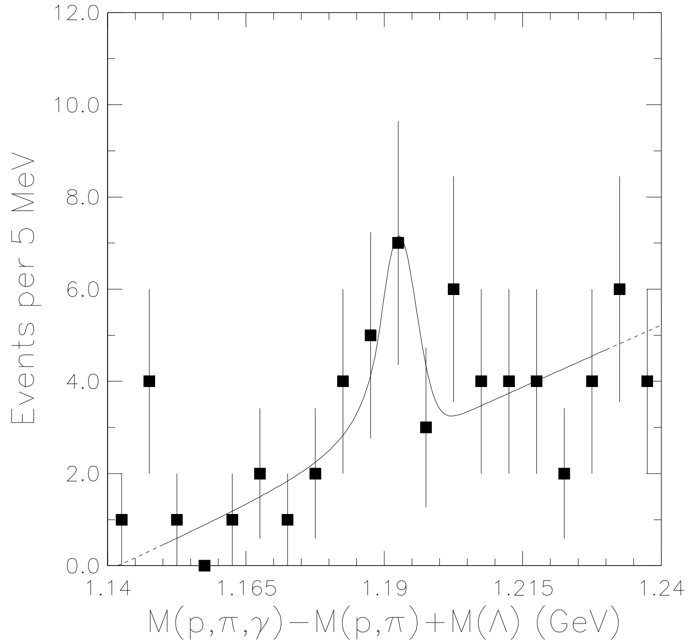

FIG. 4. Mass of $(\Sigma^o/\overline{\Sigma}^o)$, of data events

discussed further below.

We now correct the measured $e^+e^- \to e^+e^-(\Lambda/\Sigma^o)(\overline{\Lambda}/\overline{\Sigma}^o)$ cross-section using our estimate of the $\gamma\gamma \to \Sigma^o\overline{\Sigma}^o$ and $\gamma\gamma \to (\Lambda\overline{\Sigma}^o/\Sigma^o\overline{\Lambda})$ contribution to produce an uncontaminated $e^+e^- \to e^+e^-\Lambda\overline{\Lambda}$ cross-section. Due to the low statistics of the $(\Sigma^o/\overline{\Sigma}^o)$ measurement we can not determine the mixture of $\gamma\gamma \to (\Lambda\overline{\Sigma}^o/\Sigma^o\overline{\Lambda})$ and $\gamma\gamma \to \Sigma^o\overline{\Sigma}^o$. We will assume that each contributes half and assign the difference between the number given by this assumption and the assumption that all observed $(\Sigma^o/\overline{\Sigma}^o)$ events were produced by $\gamma\gamma \to \Sigma^o\overline{\Sigma}^o$ as the systematic uncertainty of the correction. Given the equal contribution assumption, to estimate the number contamination events we multiply the observed number of $(\Sigma^o/\overline{\Sigma}^o)$ by 4/3 and by the ratio of the $\Lambda\overline{\Lambda}$ finding efficiency to $(\Sigma^o/\overline{\Sigma}^o)$ finding efficiency in $e^+e^- \to e^+e^-\Sigma^o\overline{\Sigma}^o$ events. We have used the fact that the efficiency for finding $(\Sigma^o/\overline{\Sigma}^o)$ in $e^+e^- \to e^+e^-\Sigma^o\overline{\Sigma}^o$ events is approximately twice that for finding $(\Sigma^o/\overline{\Sigma}^o)$ in $e^+e^- \to e^+e^-(\Lambda\overline{\Sigma}^o/\Sigma^o\overline{\Lambda})$ events. We use this to determine the number of non-$\Lambda\overline{\Lambda}$ contamination events, $15\pm9\pm5$, and extract the exclusive $e^+e^- \to e^+e^-\Lambda\overline{\Lambda}$ cross-section of $1.3 \pm 0.4 \pm 0.6$ pb

Similarly, we correct the measured $\gamma\gamma \to (\Lambda/\Sigma^o)(\overline{\Lambda}/\overline{\Sigma}^o)$ cross-section using our estimate of the the $(\Sigma^o/\overline{\Sigma}^o)$ contamination. To a good approximation the replacement of W with $m_{\Lambda\overline{\Lambda}}$ shifts the W distribution of interest to a lower value by the difference in W threshold values between the W distribution of interest and $\Lambda\overline{\Lambda}$. Consequently, we expect the $m_{\Lambda\overline{\Lambda}}$ distribution for the observed $(\Lambda/\Sigma^o)(\overline{\Lambda}/\overline{\Sigma}^o)$ events to be a good model for the shifted $m_{\Lambda\overline{\Lambda}}$ distributions of the $\Sigma^o\overline{\Sigma}^o$ and $(\Lambda\overline{\Sigma}^o/\Sigma^o\overline{\Lambda})$ contamination. We use the shape of the $m_{\Lambda\overline{\Lambda}}$ distribution found in data to estimate the $m_{\Lambda\overline{\Lambda}}$ distribution of $(\Sigma^o/\overline{\Sigma}^o)$ contamination. This is equivalent to scaling the number of events in each bin by the factor, $f_{scale} = 1 - (15 \pm 9 \pm$

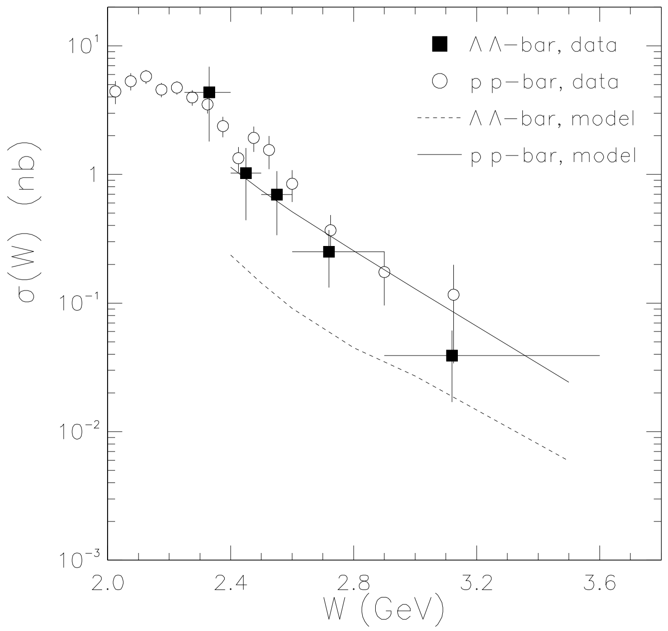

FIG. 5. $\sigma_{\gamma\gamma\to\Lambda\overline{\Lambda}}(W)$, $\sigma_{\gamma\gamma\to p\overline{p}}(W)$, $\sigma_{\gamma\gamma\to p\overline{p},model}(W)$, $\sigma_{\gamma\gamma\to\Lambda\overline{\Lambda},model}(W)$, for $|\cos\theta^*| < 0.6$, Error-bars include systematic uncertainties

$5)/48.1 = 0.69 \pm 0.19 \pm 0.10$.

Given the extracted exclusive $\gamma\gamma \to \Lambda\overline{\Lambda}$ signal, we can compare our measurement with the previously measured $\gamma\gamma \to p\overline{p}$ cross-section and with theory; see Table I and Figure 5. In Figure 5 we have placed the horizontal location of the cross-section data points at the weighted mean of $m_{\Lambda\overline{\Lambda}}$ in the bin based on a $\sim 1/W^{12}$ distribution. The interesting result is that the production of $\gamma\gamma \to \Lambda\overline{\Lambda}$ not only appears to be high compared to quark-diquark model, but appears to be at nearly the same level as $\gamma\gamma \to p\overline{p}$.

In this paper we have presented the measurement of the cross-section for $e^+e^- \to e^+e^-(\Lambda/\Sigma^o)(\overline{\Lambda}/\overline{\Sigma}^o)$ of $1.9\pm0.3\pm0.6$ pb. We also measured the $e^+e^- \to e^+e^-(\Sigma^o\overline{\Sigma}^o/\Lambda\overline{\Sigma}^o)$ contribution to this cross-section. We estimated the relative contributions of $e^+e^- \to e^+e^-\Sigma^o\overline{\Sigma}^o$ and $e^+e^- \to e^+e^-(\Lambda\overline{\Sigma}^o/\Sigma^o\overline{\Lambda})$, and extracted the exclusive $e^+e^- \to e^+e^-\Lambda\overline{\Lambda}$ cross-section of $1.3 \pm 0.4 \pm 0.6$ pb. We measured the cross-section for $\gamma\gamma \to (\Lambda/\Sigma^o)(\overline{\Lambda}/\overline{\Sigma}^o)$ as a function of $m_{\Lambda\overline{\Lambda}}$ and using the estimated $\gamma\gamma \to (\Sigma^o\overline{\Sigma}^o/\Lambda\overline{\Sigma}^o)$ contamination, we presented an exclusive $\gamma\gamma \to \Lambda\overline{\Lambda}$ cross-section. As seen in Figure 5, the measured $\gamma\gamma \to \Lambda\overline{\Lambda}$ cross-section appears to be larger than the quark-diquark model prediction. Indeed, the cross-section appears to be similar to the $\gamma\gamma \to p\overline{p}$ cross-section for values of W above threshold, although the $\gamma\gamma \to \Lambda\overline{\Lambda}$ cross-section appears to have a steeper W dependence. The large $\gamma\gamma \to \Lambda\overline{\Lambda}$ cross-section is an unexpected result.

ACKNOWLEDGEMENTS

D.W.B. thanks P. Kroll and W. Schweiger for access to their calculations. We gratefully acknowledge the effort of the CESR staff in providing us with excellent luminosity and running conditions. J.P.A., J.R.P., and I.P.J.S. thank the NYI program of the NSF, M.S thanks the PFF program of the NSF, G.E. thanks the Heisenberg Foundation, K.K.G., M.S., H.N.N., T.S., and H.Y. thank the OJI program of DOE, J.R.P, K.H., and M.S. thank the A.P. Sloan Foundation, and A.W., and R.W. thank the Alexander von Humboldt Stiftung for support. This work was supported by the National Science Foundation, the U.S. Department of Energy, and the Natural Sciences and Engineering Research Council of Canada.

REFERENCES

[1] CLEO Collaboration, M. Artuso *et al.*, *Phys. Rev. D* **50**, 5484 (1994).

[2] M. Anselmino, F. Caruso, P. Kroll, and W. Schweiger, *Int. J. Modern Phys. A.* **4**, 5213 (1989).

[3] P. Kroll, T. Pilsner, M. Schürmann, and W.Schweiger, *Phys. Lett. B* **316**, 546 (1993).

[4] Private communication with W. Schweiger (1995).

[5] CLEO Collaboration, Y.Kubota *et al. Nucl. Instr. & Meth.* **A320**, 66 (1992).

[6] D. Rubin *Proceedings of the 1995 Particle Accelerator Conference* **1**, 481 (1995).

[7] G. Farrar *et al.*, *Nucl. Phys.* **B259**, 702 (1985); **B263**, 746(E) (1986).

[8] V.M.Budnev, I.F.Ginzburg, G.V.Meledin, and V.G.Serbo, *Phys. Rep.* **15C**, 181 (1975).

[9] R.Brun *et al.*, "GEANT3 Users Guide," CERN DD/EE/84-1 (1987).